Hindawi
Geofluids
Volume 2022, Article ID 5033658, 12 pages
https://doi.org/10.1155/2022/5033658

Research Article

Influence of Lower Double-Track Tunnel Spacing on the Stress and Deformation Characteristics of Upper Tunnel in Double-Level Condominium Tunnels

Huang Zhanjun,[1] Guo Wanglong,[2,3] Tong Lihong,[2,3] He Xiaohui,[1] Ding Haibin,[2,3] and Li Songyan[4]

[1]*Nanchang Rail Transit Group Limited Corporation, Nanchang, 330013 Jiangxi, China*
[2]*School of Civil Engineering and Architecture East China Jiaotong University, Nanchang 330013, China*
[3]*Engineering Research & Development Centre for Underground Technology of Jiangxi Province, Nanchang 330013, China*
[4]*China Construction Fourth Engineering Division Corp. LTD, Guangzhou 510665, China*

Correspondence should be addressed to Tong Lihong; lhtong@ecjtu.edu.cn

Received 9 May 2022; Revised 26 May 2022; Accepted 9 June 2022; Published 3 July 2022

Academic Editor: Dongjiang Pan

The open-cut tunnels in Aixi Lake, Nanchang, are constructed in a condominium form of highway tunnel and subway tunnel, which are the first superimposed double-level tunnels in China. The scientific problems faced by this new structure form have attracted the attention of engineers and researchers. If this structure form can be reasonably used, it can reduce the repeated excavation of the ground and reduce the impact of highway tunnel construction on subway tunnels. It is of great guiding significance to study the influence of the spacing between lower double-track subway tunnels on the stress and deformation characteristics of the upper highway tunnel. Based on the model test, the deformation, axial force, bending moment, and earth pressure of the upper highway tunnel are studied. The results show that the maximum displacement of upper tunnel floor can be reduced by 30% when the spacing of the lower tunnel makes the center line of the lower single tunnel coincide with the quadripartite line of the upper tunnel. Horizontal spacing between lower double-track tunnels significantly influences the bending moment of upper tunnel floor but hardly influences the axial force of the upper tunnel floor. Considering the influence of lower tunnel spacing on the earth pressure of the upper tunnel floor, the spacing of the lower tunnel should not exceed 50% of the section width of the upper tunnel.

1. Introduction

With the acceleration of urbanization, the construction of subway tunnels and highway tunnels is gradually strengthening in China [1, 2]. To alleviate the overexploitation of underground space, the double-level condominium tunnels with a structural form of the lower double-track subway tunnels and the upper road tunnel were adopted [3]. The research on public double-level condominium tunnels in China is still insufficient. Moreover, the stress characteristics and deformation trend of the upper road tunnel are not clear when the horizontal spacing between the lower double-track tunnels changes. Related specifications clearly stipulate that the spacing between tunnels is at least twice as large as the tunnel diameter [4–6]. However, at present, no specific reasonable spacing is available. Determining a reasonable horizontal spacing between the lower double-track tunnels can optimize structure form of the public double-level condominium tunnels, which has great guiding significance for the construction of such tunnels.

Regarding the reasonable horizontal spacing between lower double-track tunnels [7, 8], scholars have conducted numerous in-depth studies and achieved many meaningful conclusions. Based on numerical simulation, Li et al. [9] gave some suggestions for the determination of reasonable spacing of horizontal and longitudinal overpass tunnels on

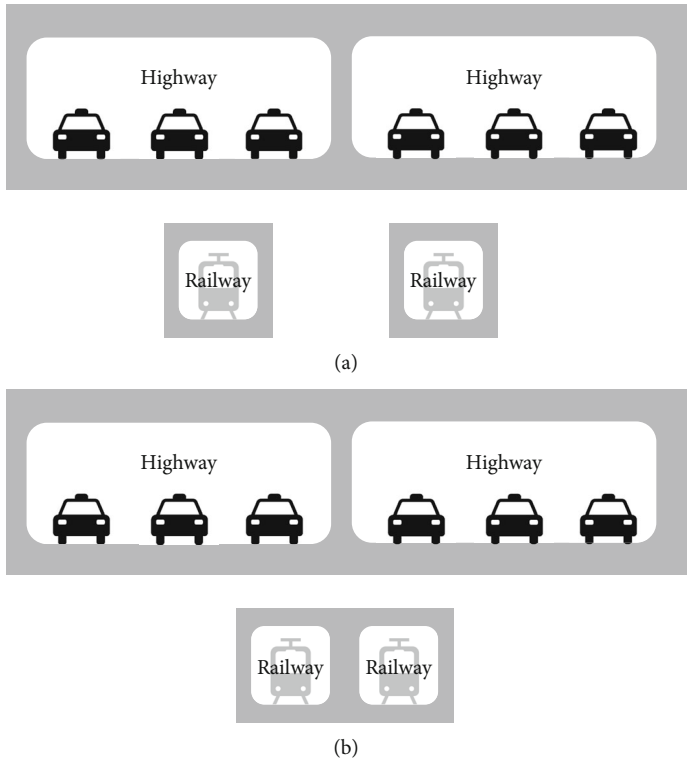

Figure 1: Structural form of Aixi Lake tunnel: (a) the west and east parts of the tunnel and (b) the middle part of the tunnel.

urban underground roads. Wang et al. [10] provided the best combination of spacing and flatness rate of large cross-section small net distance tunnels under engineering conditions by using the large finite element analysis software ABAQUS. Liu et al. [11] combined theoretical derivation and numerical simulation to analyze the safety spacing and layout of the three-hole tunnels and obtained the influence of the three-hole tunnels on surface settlement. Song et al. [12] used the complex variable functions to establish a mechanical model of adjacent horizontal tunnels in combination with the D-P yield criterion, so as to calculate the reasonable tunnel spacing. In summary, these existing studies pay more attention to the impact of the horizontal spacing of lower double-track tunnels on the surface settlement or the tunnel itself [13, 14]. The influence of the horizontal spacing between the lower double-track tunnels on the stress and deformation characteristics of the upper tunnel floor has not yet been studied.

Nowadays, model experiment is one of the important methods for tunnel researches. Generally, given the main physical quantities affecting the force or deformation of the tunnel, whether the mathematical equations of the problem needed to be studied can be listed or not; model experiments are applicable to obtain practical research results [15]. Wei et al., Zhang et al., Xu et al., and Gan et al. [1, 14, 16, 17] all carried out tunnel structure model tests based on actual projects and provided valuable references for tunnel constructions. However, most of these research objects focused on the single-layer shield tunnels and road tunnels [18]. The impact of horizontal spacing between double-track tunnels on the upper tunnel in double-level condominium tunnels was rarely reported [19].

Based on the Nanchang Aixi Lake Tunnel Project, in this study, a model test system for the deformation of the upper tunnel floor caused by the change of horizontal spacing between the double-line tunnels was established. The deformation and force laws of the upper tunnel floor under the condition of different horizontal spacings of the lower double-track tunnels were analyzed. The research results can provide certain references and suggestions for determining a reasonable horizontal spacing between the lower double-track tunnels in double-level condominium tunnels.

2. Engineering Background

The total length of Nanchang Aixi Lake public railway tunnel is about 2664 m, in which the length of highway and subway superimposed tunnels is 2280 m. The project is composed of a two-way six-lane highway tunnel in the upper level and the lower double-line tunnels on Nanchang Metro Line 3. The bottom plate of superstructure and the top plate of lower structure are in the form of a noncommon board. The horizontal spacing between tunnels in the west and east Aixi Lake is different from that in the middle of Aixi Lake, as shown in Figure 1. The two upper-level tunnels are 28.9 m wide and 8 m high with a rectangular middle wall between them. On the lower level are two separate rectangular tunnels with a width of 6 m and a height of 6.7 m. The specific parameters of a typical tunnel section are shown in Figure 2. According to the engineering survey data of Aixi

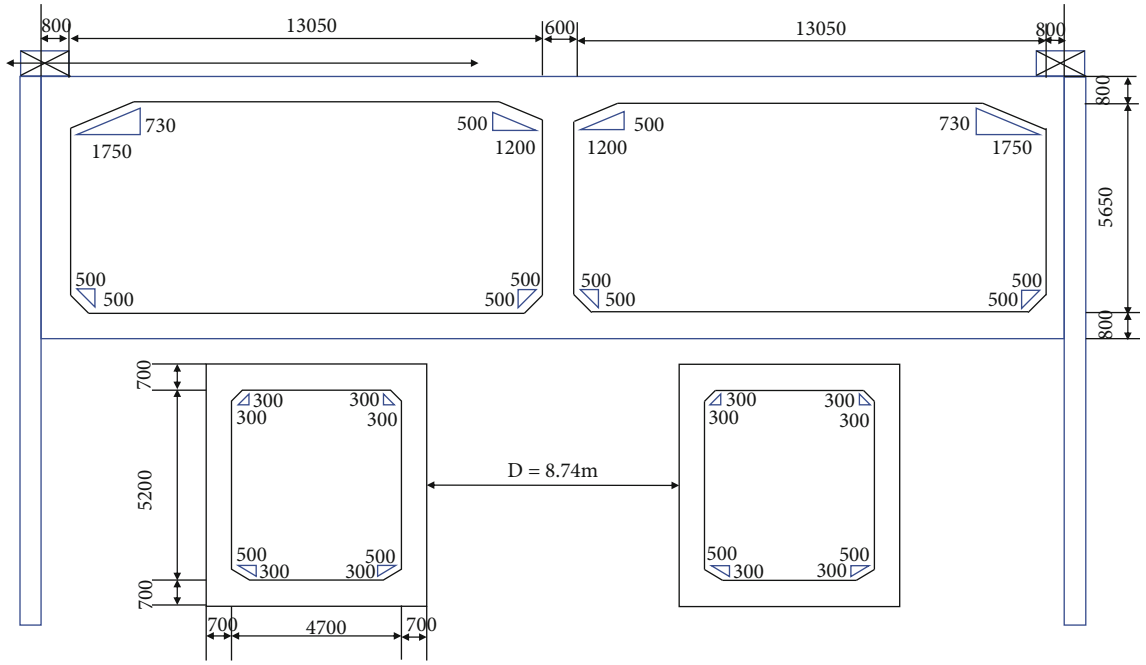

Figure 2: Specific parameters of a typical section of Aixi Lake tunnel.

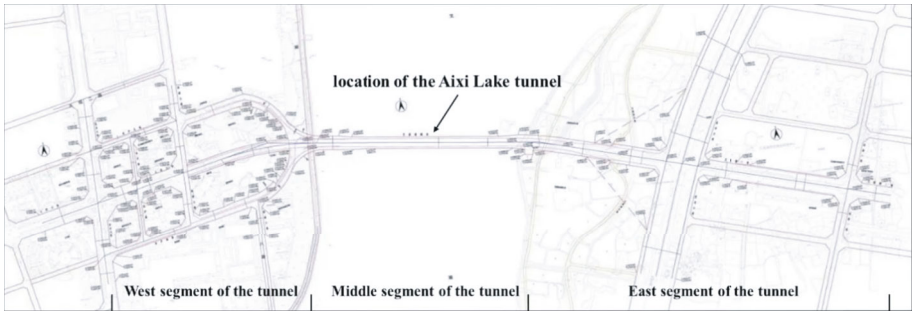

Figure 3: The location map of the Aixi Lake tunnel.

Lake, the upper tunnel and the lower tunnel are both quaternary loose sediments in the depth range, mainly composed of water-rich sand layers. Figure 3 is the location map of the Aixi Lake tunnel.

3. Physical Model Experiment

To investigate the influence of lower tunnel horizontal spacing on the deformation and stress characteristics of upper tunnel floor, a reduced scale model experiment with a geometric similarity ratio of 1 : 30 was performed. The earth pressure of the upper tunnel floor was measured by an earth pressure cell, and the full-field strain and displacement of the bottom plate of upper tunnels were measured by the VIC 2D noncontact full-field strain measurement system.

3.1. Geometric Similarity Ratio. For a tunnel model, it is necessary to first determine the geometric similarity conditions. Factors such as the model type, material, loading capacity, and equipment conditions should be considered so as to determine an appropriate geometric similarity constant.

Table 1: Similarity table.

Physical quantities	Symbol	Similarity ratio
Tunnel size	L	30
Bulk weight	γ	1
Strain	ε	1
Elastic modulus	E	30
Axial force	N	30^3
Shear force	Q	30^3
Deformation	s	30

In this experiment, the model was limited to the elastic deformation range of the material, and the resulting stress generally conforms to the elastic theory. That is, an elastic model was established. In addition, the reference value of the geometric similarity constant c_l of the elastic model of the rectangular tunnel structure is 20-40.

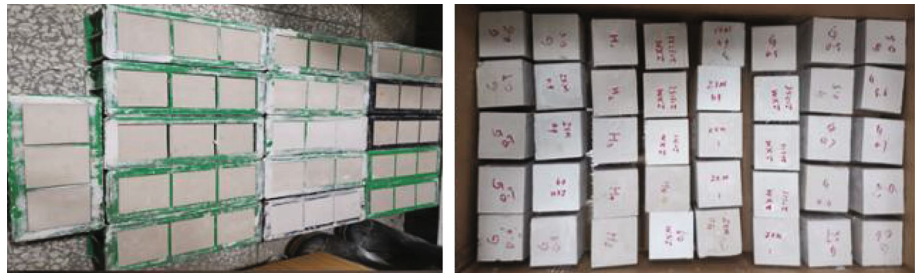

Figure 4: Production and maintenance of cube samples with different proportions.

Combining the similarity theory and elastic mechanics, the geometric similarity ratio of the reduced scale model is determined as 1 : 30.

3.2. Determination of Similarity Constant. From the basic criterion of similarity theory, for a static elastic stress model, the physical quantities involved in this experiment include the geometric dimension l, bulk weight γ, strain ε, stress σ, axial force N, shear force T, and elastic modulus EI. On the basis of determining the geometric similarity constant $c_l = 30$ and the bulk weight similarity constant $c_\gamma = 1$, the above physical quantities can be determined according to the similarity criterion and dimensional analysis method, as listed in Table 1.

3.3. Similar Materials. Due to the wide variety of model materials, it is difficult to find an absolutely ideal one. Therefore, when selecting model materials to simulate the tunnel structure, it is necessary to fully understand the performance, advantages, and disadvantages of the model materials for a reasonable selection. Moreover, the performance of the selected model material should meet the requirements of similar conditions proposed in the model design. It also should be ensured that the test material has sufficient linear elastic properties within the test range. The prototype structure in this model test is the reinforced concrete rectangular tunnel of C40, while the elastic modulus of C40 concrete is 3.25 GPa. The elastic modulus of similar materials should be close to 1/30 of 3.25 GPa, that is, 1080 MPa.

Considering the above factors, gypsum was selected as the similar material of tunnel structure. The physical properties of gypsum are similar to those of concrete. Gypsum is a brittle material with an elastic modulus of 1000-5000 MPa and is easy to process and fast to molding. At present, the use of gypsum models in concrete structures is more common. In a gypsum model, gypsum serves as the basic cementing material. The physical properties of gypsum mixture can be adjusted by adding admixtures. The elastic modulus of a gypsum model can be determined by adjusting the proportions of admixture, gypsum, and water. For an accurate strain measurement, the maximum particles of the external feeding should be limited. Therefore, diatomaceous powder with a particle size of less than 1 mm is used in this model.

To control the elastic modulus of the gypsum model close to a theoretical value, this paper conducts a material ratio test with different proportions of water, gypsum, and diatomaceous. As is shown in Figure 4, by making cube specimens (70.7 mm × 70.7 mm × 70.7 mm) with different proportions of water, gypsum, and diatomaceous powder, uniaxial compression tests were conducted. Specimens were maintained under standard maintenance conditions for 28 days. The uniaxial compressive strength and elastic modulus of the materials with different proportions of water, gypsum, and diatomaceous powder are summarized in Table 2.

Table 2: Material ratio and properties of gypsum model.

Water : gypsum : diatomite	Uniaxial compressive strength (MPa)	Elasticity modulus (MPa)
2 : 1 : 1.1	2.25	1771
2 : 1 : 1.0	2.11	1560
2 : 1 : 0.9	1.75	1374
2 : 1 : 0.8	1.52	1200
2 : 1 : 0.7	1.42	1125
2 : 1 : 0.6	1.38	966
2 : 1 : 0.5	1.31	870

From Table 2, it can be seen that when the mass ratio of water, gypsum, and diatomaceous powder is 2 : 1 : 0.7, the elastic modulus and uniaxial compressive strength are 1.42 MPa and 1125 MPa, respectively, with a difference relative to the required value less than 5%. Therefore, this mass ratio can be used for the model experiment.

3.4. Experimental Apparatus. The experimental apparatus mainly includes two parts: the model system and the data acquisition system. Figure 5 illustrates a flowchart of the experimental apparatus.

3.4.1. Model System. The model system mainly includes the model box, the lower double-track subway tunnel model, and the upper tunnel model. The main role of the model box is to fill sand used for the model test and bear the tunnel model. The length, width, and height of the model box are 1.74 m, 1.74 m, and 1.2 m, respectively, and surroundings of the model box are reinforced with thickened plexiglass, which allows a real-time observation during experiments. Meanwhile, a square hole is prepared on the side of the model box, whose size is slightly larger than that of the upper tunnel. This provides the convenience for the VIC strain measurement system to collect data. In order to

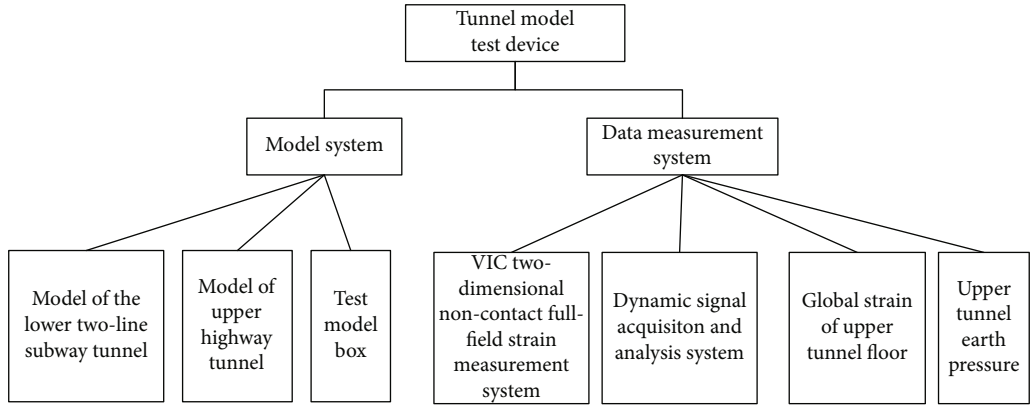

Figure 5: Composition diagram of test device.

Table 3: Physical parameters of sand.

Physical index	Bulk weight γ (kN/m^{-3})	Void ratio	Water cut (%)	Internal friction angle (°)	Compression modulus (MPa)
Numerical value	16.5	0.582	5.26	31.2	30.3

reduce the boundary effects, lubricant can be applied to reduce the friction between sand and the plexiglass wall before the model box is filled with sand.

The upper and lower tunnel models are made by pouring a mixture of gypsum, water, and diatomaceous powder in the formwork, and the steel cages in prototype tunnels are replaced by steel wire mesh according to the principle of the equal reinforcement rate. Steel wire mesh mainly plays a role of tensile resistance in gypsum, and because of its own properties, it can play a synergistic effect with gypsum. Asbestos mesh is added to enhance the overall performance of the gypsum model. The section size of the tunnel model is a 1/30 scale reduction of that illustrated in Figure 2, with a length of 600 mm. The whole gypsum model is made of three tunnel models with a length of 200 mm using AB glue. Because the gypsum model is extremely susceptible to moisture, three layers of waterproof are brushed on the outside of the tunnels. After the paint solidifies, a protective waterproof is formed, which is tested to have no effect on the stress and deformation of the model.

In this model experiment, sand from the Ganjiang River was sieved through a 5 mm sieve. The basic physical and mechanical indicators of the sand are determined and shown in Table 3. The density of river sand can be controlled by layered filling of test soil and compaction with vibrator.

3.4.2. Data Measurement System. The test system is mainly composed of the VIC two-dimensional noncontact full-field strain measurement system and the dynamic signal acquisition and analysis system. As shown in Figure 6, the VIC two-dimensional noncontact full-field strain measurement system consists of an industrial camera and a light source. By coating the model surface to be measured with appropriately sized scattered speckle and using the industrial camera to shoot a large number of images of the model surface at a set frequency, the full-field strain and displacement of the model surface can be obtained after processing the filmed images with a data analysis software. The dynamic signal acquisition and analysis system is mainly used to measure the earth pressure around a tunnel (Figure 7). After the earth pressure box is arranged at each measurement location, the wire is connected to the dynamic signal acquisition analyzer and then connected to the computer through a network cable. The experimental data are obtained and processed through a data software in the computer. To ensure that the data measurement system works properly, a 5 min trial test is conducted before the formal experiment.

3.5. Simplification of Experiments. Considering the experimental operability and the particularity of the VIC measurement system, this paper simplifies the model experiment.

(1) The upper- and lower-level tunnels are, respectively, constructed in sections in the actual project. In this test, the tunnel model is made by separate sections with a length of 200 mm, and thus, a partial structure is simplified. The segmented tunnels are connected to each other as a whole by AB glue whose adhesive strength can reach 12 MPa, which can fully ensure the integrity of the tunnel model

(2) Since most of the tunnel structures in the actual project is embedded in the same soil layer, here, the model soil is simplified to a uniform soil layer and only one soil is used

3.6. Arrangement of Measurement Locations. To study the earth pressure distribution characteristics of upper- and lower-level tunnels, we arranged 6 measuring locations with equal spacing on the upper tunnel, as shown in Figure 8. Because the VIC strain system can measure a full-field strain, we only need to uniformly coat the model surface

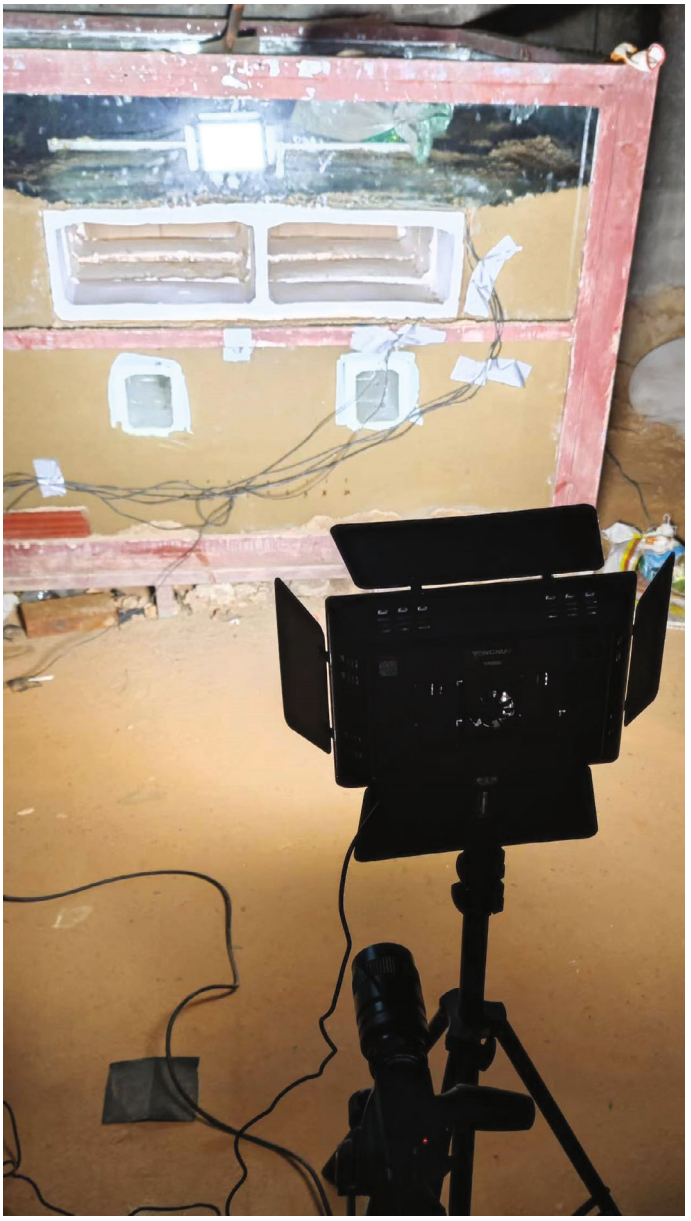

Figure 6: VIC two-dimensional noncontact full-field strain measurement system.

where strain measurement is desired with speckle like Figure 9.

3.7. Test Conditions. The main research object in this paper is the spacing between the lower double-track subway tunnels. Referring to the Aixi Lake tunnel with the maximum spacing of 8.75 m, the model spacing was determined as 30 mm according to the similarity first principle. In addition, according to the actual project, the distance between the upper- and lower-level tunnels was set as 10 mm. Setting 30 mm as D, the following five test conditions with the spacings of 0, $1/3D$, $2/3D$, D, and $4/3D$ were designed. The test condition with 0 spacing was based on the fact that the double-track tunnels at the lower level were merged into a single two-hole tunnel in the actual project. The detailed test conditions are described in Table 4.

Figure 7: Dynamic signal acquisition and analysis system.

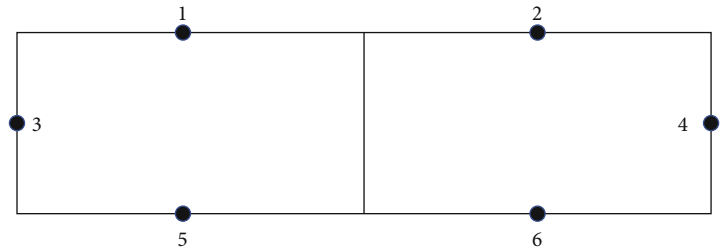

Figure 8: Earth pressure measuring point layout of upper tunnel.

3.8. Experimental Procedure

(1) *Monitoring Layout*. Earth pressure cells were pasted at the determined measuring locations in the upper highway tunnel model according to the specifications. The DHDAS dynamic signal acquisition and analysis software was used to judge whether each earth pressure cell can work normally. Spot speckle on the model surface of the upper highway tunnel that needs to be measured was evenly created using a black marker. The size of speckle is calculated according to the monitoring requirements of the VIC measurement system.

(2) *Waterproof Treatment*. Joints between the tunnel model blocks were bonded with waterproof tape to prevent the water in the sand from infiltrating the tunnel joints.

(3) *Experimental Preparation*. Surroundings of the model box frame were with transparent tempered glass. Vaseline was applied on the sides to reduce the influence of boundary effects. For a convenient operation of the subsequent experiment, the height of the upper- and lower-level tunnels and the spacing under the five test conditions were drawn on the model box.

(4) *Sand Filling*. The same amount of sand was poured into the model box using the falling rain method at the same height. Sand pouring was stopped until the height of the sand reaches the bottom of the lower tunnel, and the sand was compacted. The lower double-track tunnel model was arranged horizontally according to the spacing under the first test condition. The gap between the tunnel and the tempered glass was sealed with water-stop tape. Sand filling continued until the height of the sand reached the bottom of the upper tunnel. Subsequently, the upper tunnel model is placed horizontally.

(5) *Equipment Debugging*. When the top of the upper tunnel was not buried with sand, setting up of the industrial camera and light source of the VIC measurement system was started. Ten images were filmed for preprocessing to ensure the normal operation of the equipment. Meanwhile, the earth pressure cells pasted to the upper tunnel were connected with the computer to observe if signal channels were normal. In the measurement process of the VIC system, it is necessary to ensure that the distance between the industrial camera and the speckle of the tunnel cross-section meets the requirements of the equipment and that the light of the whole environment does not change during the photography process, so as to avoid the influence of the process involved in the preparation and testing on the observation of the speckle.

Figure 9: Speckle diagram of upper tunnel.

Table 4: Test conditions.

Test no.	Spacing between lower double-track tunnels (cm)	Distance between the upper and lower tunnels (mm)
1	0	10
2	10	10
3	20	10
4	30	10
5	40	10

(6) *Data Collection*. Data of global strain and earth pressure at measuring locations were collected when filling sand above the upper tunnel. When sand was poured until the top of the model box, the sand was desired to consolidate, and the data capture began. After the data were stabilized and standing for 12 h, data collection under the first test condition was finished.

(7) *Experimental Repetition under Different Test Conditions*. The measuring device was zeroed out, and the model box was cleaned up after the experiment under a given test condition. The test components, sand, and tunnel model were sorted out for the experiments under other test conditions. The experiment following each test conditions was carried out in strict accordance with the same steps as above, so

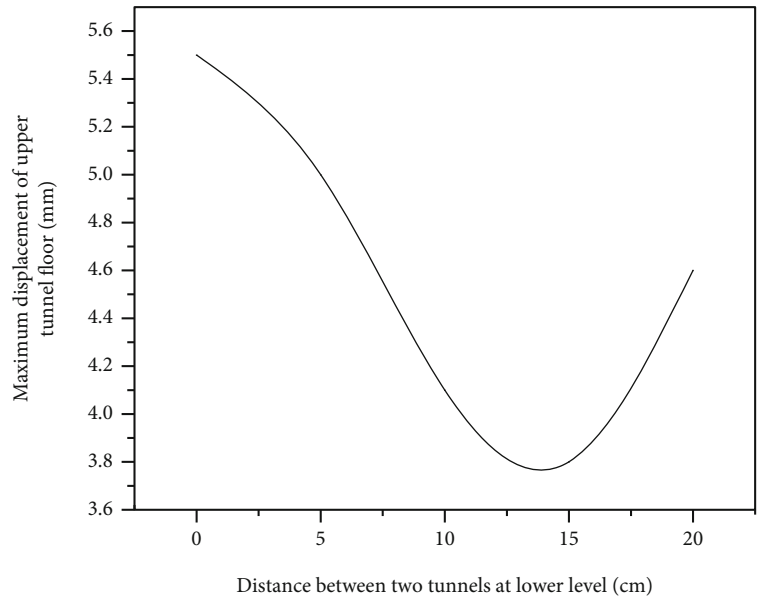

Figure 10: Maximum displacement of upper tunnel floor at different spacings.

as to avoid errors caused by differences in operating steps.

4. Results and Discussion

4.1. Deformation Analysis of Upper Tunnel Floor. When the data collected by the VIC measurement system stabilized, the full field displacement of the area covered with speckle in upper- and lower-level tunnels can be obtained. This paper focuses on the influence of horizontal spacing between the lower double-track tunnels on the upper tunnel floor; only the floor displacement of the upper tunnel model was analyzed in this section.

Figure 10 shows the changes in the maximum displacement of the upper tunnel floor with the spacing between the lower double-track tunnels. It can be seen that the maximum displacement of the upper tunnel floor reaches 5.7 mm when the lower tunnel spacing is 0. As the lower tunnel spacing gradually increases to D, the maximum displacement decreases gradually. However, when the lower tunnel spacing further expands to $4/3D$, the maximum displacement increases again.

Figure 11 shows the displacement curves of the upper tunnel floor under different lower double-track tunnel spacings (in view of the symmetry, the left half displacement of the upper floor serves as the abscissa). It is observed that the changes in the lower tunnel spacing not only affect the magnitude of the peak displacement but also influence the location where the displacement peaks. In the range of $0 - D$ spacing, the location of the peak displacement is gradually away from the symmetry axis. In contrast, when the spacing increases to $4/3D$, the location of peak displacement approaches the symmetry axis. In addition, the location of peak displacement fluctuates between 200 mm and 300 mm away from the symmetry axis (that is, near the central axis of the left half of floor).

Combined with Figures 10 and 11, it is found that the lower tunnel spacing significantly influences the peak displacement of the upper tunnel floor and its occurrence location. When the spacing is D, the peak displacement is the smallest. This is because when the lower double-track tunnel spacing is D, the spacing of the lower tunnel makes the center line of the lower single tunnel coincide with the quadripartite line of the upper tunnel. In this case, an optimal support for the maximum displacement point of the upper tunnel is achieved, thus reducing the displacement of the upper tunnel by 30%. Also, the relative location of the maximum displacement point was adjusted.

4.2. Internal Stress Analysis of Upper Tunnel Floor. In the experiment, the upper tunnel floor is mainly stressed by the tunnel self-weight, vertical earth pressure, lateral earth pressure, and soil friction. Hereinafter, the axial force and bending moment of the upper tunnel floor were analyzed. In the software supporting the VIC measurement system, the corresponding bending moment and axial force can be directly obtained by using the collected strain data.

It is seen from Figure 12 that the axial force of the upper tunnel floor is slightly affected by the lower tunnel spacing. In particular, at the side wall (location A in Figure 12) and the middle wall (location C in Figure 12), the change rate of the axial force at the side wall is all within 4%, and that at the side wall fluctuates around 5%. However, in the middle location of the tunnel (location B in Figure 12), axial force is greatly affected by the lower tunnel spacing. The change rate of axial force decreases from 6% to 4% as the spacing increases. These observations indicate that changing the lower double-track tunnel spacing has little effect on the axial force of the upper tunnel floor, especially at the side wall and middle wall.

Figure 13 depicts the bending moment curve of the upper floor under different lower double-track tunnel

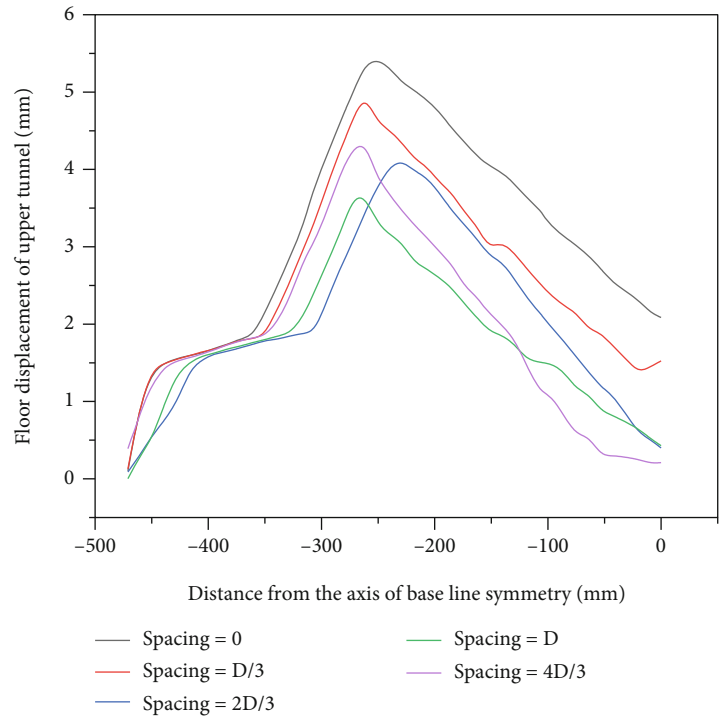

Figure 11: Displacement curve of upper tunnel floor.

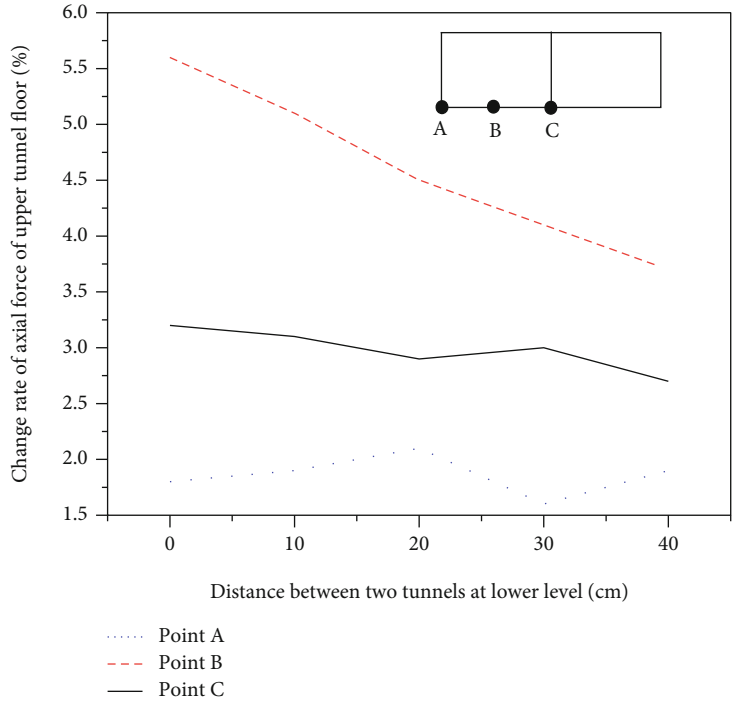

Figure 12: Change rate of axial force of upper floor under different spacings.

spacings. The overall bending moment presents a "W"-shaped distribution. The maximum positive bending moment occurs in the interval of 200-300 mm from the central axis. The reason is that the weakest area of the floor occurs in the central area of the upper tunnel, which is greatly affected by the overburden. As the spacing gradually increases from 0 to D, the difference between the positive and negative bending moments continuously decreases. The bending moment curve under $4/3D$ is similar to that under $D/3$. This finding implies that when the distance is

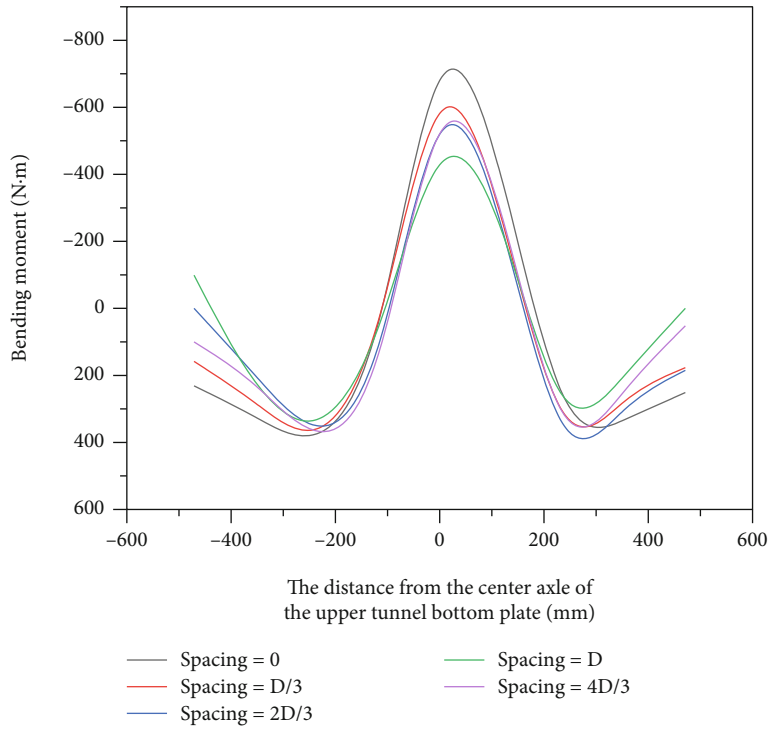

Figure 13: Bending moment curve of upper tunnel floor.

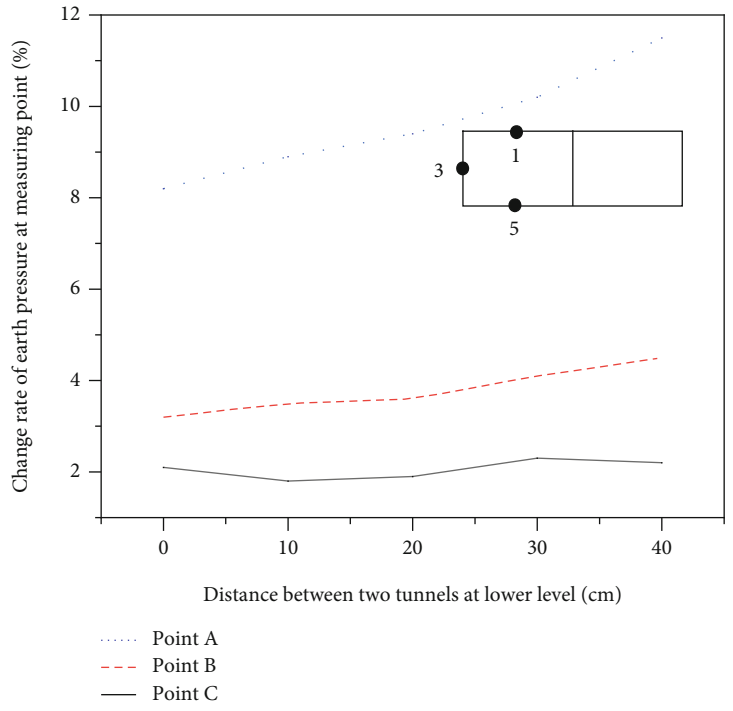

Figure 14: Change rate of axial force of upper floor under different spacings.

D, the stress condition of the upper tunnel floor is desired, and in such condition, the maximum bending moment can be reduced by 40%. This adjustment can be seen as a way to adjust the bending moment of the bottom plate by adjusting the bearing of the plate. Therefore, the influence of the lower tunnel spacing on the bending moment of the upper tunnel floor is greater than that of the axial force and should be a major concern in tunnel design.

4.3. Earth Pressure Analysis of Upper Tunnel. In this experiment, six measuring locations (Figure 8) were selected for collection of earth pressure data. Among them, the measuring locations 1, 3, and 5 and the measuring points 2, 4, and 6 were symmetrically distributed. The measuring locations 2, 4, and 6 were functioned as the control group for a comparison with the data from measuring locations 1, 3, and 5.

Figure 14 shows the relationships between the variation rate of earth pressure at measuring points 1, 3, and 5 and the spacing between lower double-track tunnels. It can be seen that the distance between the upper and lower tunnels has little effect on the earth pressure of side wall (location 3) and roof (location 1), and the change rate is within 5%. However, with an increase in the spacing, a relatively large impact on the soil pressure of the floor is observed. Therefore, considering the influence of uneven distribution of soil pressure on floor displacement, the horizontal spacing between the lower tunnels should not be too large.

5. Conclusions

Based on the Aixi Lake Tunnel project, indoor model experiment of the double-level condominium tunnels was conducted in this study. The main conclusions are as follows:

(1) It is considered that the most rational spacing between the lower double-track tunnels is D, which can reduce the maximum floor displacement by 30%. In the actual construction, it is suggested to make the central axis of a single lower tunnel close to the quadripartite line of an upper tunnel. This measure can control the deformation of the upper tunnel

(2) The spacing between the lower double-track tunnels has a great influence on the bending moment of the upper tunnel floor and a small influence on the axial force. When the spacing ranges in $0 - D$, the maximum bending moment decreases with the increase of spacing. When the spacing exceeds D, the maximum bending moment increases. Compared with that of 0 spacing, the maximum bending moment of bottom plate with D spacing is reduced by 40%. Therefore, by adjusting the spacing between the lower double-track tunnels, the bending moment distribution of the bottom plate can be adjusted, and the optimal stress position can be achieved

(3) The earth pressure of the upper tunnel floor increases with the spacing between the lower double-track tunnels. The greater the spacing, the greater the increment of earth pressure. An uneven increase of earth pressure can cause the increase of floor bending moment. Thus, the lower tunnel spacing should be as small as possible in practical engineering

(4) In the following work, the research will focus on the influence of the distance between the upper tunnel and the lower tunnel on the upper tunnel and will be studied by combining numerical simulation and model test, so as to further study the stress and deformation characteristics of this new kind of tunnel structure

Data Availability

Data are available from Lihong Tong (lhtong@ecjtu.edu.cn) for researchers.

Conflicts of Interest

The authors declare that there are no conflicts of interest regarding the publication of this paper.

Acknowledgments

This work was supported by the Nanchang Rail Transit Group scientific research project (2019HGKYB002), the Natural Science Foundation of Jiangxi Province (Grant No. 20192ACB20001), the National Science Fund of China (Grant Nos. 51878276 and 52108321), and the Natural Science Foundation of Jiangxi Province (Grant Nos. 20202ACB211002 and 20212BAB204012).

References

[1] Z. G. Zhang, Z. X. Cheng, J. Chen, Z. T. Wu, and Y. Z. Li, *Model test on deformation of existing pipeline induced by joint leakage of shield tunnels*, Hazard Control in Tunnelling and Underground Engineering, 2022.

[2] X. Wang, J. Li, X. Zhao, and Y. Liang, "Propagation characteristics and prediction of blast-induced vibration on closely spaced rock tunnels," *Tunnelling and Underground Space Technology*, vol. 123, article 104416, 2022.

[3] D. L. Wang, "An brief analysis of the design of large span cavern group with road and rail transit overlapped section," *Technology of Highway and Transport*, vol. 34, no. S1, pp. 147–153, 2018.

[4] L. Qiu, Y. Zhu, D. Song et al., "Study on the nonlinear characteristics of EMR and AE during coal splitting tests," *Minerals*, vol. 12, no. 2, p. 108, 2022.

[5] D. J. Pan, K. R. Hong, H. L. Fu, J. Zhou, N. Zhang, and G. Lu, "Influence characteristics and mechanism of fragmental size of broken coal mass on the injection regularity of silica sol grouting," *Construction and Building Materials*, vol. 269, p. 121251, 2021.

[6] D. J. Pan, K. R. Hong, H. L. Fu, J. Zhou, and N. Zhang, "Experimental study of the mechanism of grouting colloidal nano-silica in over-broken coal mass," *Quarterly Journal of Engineering Geology and Hydrogeology*, vol. 54, no. 4, pp. qjegh2020–qjegh2161, 2021.

[7] W. S. Wei, "Discussion on the reasonable spacing of shallow, unsymmetrical loading and closely-spaced tunnel," *Journal of Hunan University of Arts and Science (Natural Science Edition)*, vol. 25, no. 4, pp. 64–69, 2013.

[8] L. Yan, C. H. Liu, S. H. Yu, S. Wen, and H. T. Yang, *Combined pressure arch test and numerical analysis of surrounding rock in nearby twin-tunnels*, Journal of Beijing Jiaotong University, 2022.

[9] P. F. Li, F. Wang, C. P. Zang, S. P. Qin, and X. Nie, "Study on the reasonable spacing and enhanced support zone for the interchange tunnels of an urban underground road," *Modern Tunnelling Technology*, vol. 52, no. 6, pp. 111–117, 2015.

[10] H. Wang, W. Z. Chen, P. S. Chen, H. M. Tian, J. J. Cao, and W. S. Zhao, "Study of section morphology and reasonable distance optimization of large-span twin tunnels with small clear spacing in shallow rock mass," *Rock and Soil Mechanics*, vol. 32, no. S2, pp. 641–646, 2011.

[11] N. Liu, Y. X. Huang, W. Cai, and K. Chen, "Analysis of ground settlement on safety spacing and excavation length of triangle tunnel," *Journal of Huazhong University of Science and Technology*, vol. 49, no. 5, pp. 98–103, 2021.

[12] W. C. Song, Y. T. Gao, S. C. Wu, Q. Yan, and Q. L. Wu, "Reasonable spacing of parallel tunnels based on the complex function theory and D–P yield criterion," *Chinese Journal of Engineering*, vol. 38, no. 2, pp. 291–298, 2016.

[13] Z. Wen, O. Y. Jian, D. X. Yang, X. J. Wang, Z. Q. Guo, and K. J. Hu, "Effect of the in situ leaching solution of ion-absorbed rare earth on the mechanical behavior of basement rock," *Journal of Rock Mechanics and Geotechnical Engineering*, vol. 13, 2022.

[14] H. Wu, G. Y. Zhao, and S. W. Ma, "Failure behavior of horseshoe-shaped tunnel in hard rock under high stress: phenomenon and mechanisms," *Transactions of Nonferrous Metals Society of China*, vol. 32, no. 2, pp. 639–656, 2022.

[15] H. X. Wang, W. Liu, K. P. Gu, and J. T. Zhang, "Design and manufacture of waterproof quasi-prototype test model on main structure of under lake tunnel," *Construction & Design for Engineering*, vol. 17, pp. 56–58, 2021.

[16] T. Q. Xu and S. G. Li, *Research on influence of reverse fault dislocation on tunnel structure*, Railway Standard Design, 2022.

[17] X. Q. Gan, M. Zeng, H. You, D. X. Yu, P. Li, and J. L. Chen, "Study on shaking table test of mountain tunnel under fault dislocation and earthquake action," *South China Journal of Seismology*, vol. 41, no. 3, pp. 8–17, 2021.

[18] J. P. Li, Z. M. Chen, and Z. W. Xue, "Research on large deformation model test of plate-like soft rock with high ground stress," *Modern Tunnelling Technology*, vol. 59, no. 1, pp. 164–175, 2022.

[19] M. M. He, Z. Q. Zhang, J. W. Zhu, N. Li, G. Li, and Y. S. Chen, "Correlation between the rockburst proneness and friction characteristics of rock materials and a new method for rockburst proneness prediction: field demonstration," *Journal of Petroleum Science and Engineering*, vol. 205, article 108997, 2021.